Chinese Chemical Letters 37 (2026) 111416

Contents lists available at ScienceDirect

Chinese Chemical Letters

journal homepage: www.elsevier.com/locate/cclet

Controllable syntheses of {SbW_9O_{33}}-sandwiched silver clusters induced by external phosphine ligands towards 4-nitrophenol reduction

Wanting Sun, Lan Deng*, Mengyun Zhao, Tianfu Liu*, Hongjin Lv*

MOE Key Laboratory of Cluster Science, Beijing Key Laboratory of Photoelectric/Electrophotonic Conversion Materials, School of Chemistry and Chemical Engineering, Beijing Institute of Technology, Beijing 102488, China

ARTICLE INFO

Article history:
Received 17 April 2025
Revised 28 May 2025
Accepted 6 June 2025
Available online 6 June 2025

Keywords:
Polyoxometalates
Silver nanoclusters
Photoluminescence
Photothermal conversion
4-Nitrophenol reduction

ABSTRACT

In this work, we report the controllable synthesis and characterization of four atomically precise silver clusters, $Ag_{18}(SbW_9O_{33})_2(DPPP)_8$ (**1**, DPPP = 1,3-bis(diphenyphosphino)propane), $Ag_{18}(SbW_9O_{33})_2(DPPB)_8$ (**2**, DPPB = 1,4-bis(diphenylphosphino)butane), $Ag_{18}(SbW_9O_{33})_2(DPPPe)_8$ (**3**, DPPPe = 1,5-bis(diphenylphosphino)pentane), and $Ag_{18}(SbW_9O_{33})_2(TPP)_{14}$ (**4**, TPP = triphenylphosphine) by using a facile one-pot solvothermal approach. The resulting four Ag clusters exhibit similar lacunary $[SbW_9O_{33}]^{9-}$ ({SbW_9O_{33}})-sandwiched structures, which can be adjusted by the external different phosphine ligands. In addition, all four clusters display variable physicochemical and catalytic performance, correlating well to their distinct molecular structures.

© 2026 Published by Elsevier B.V. on behalf of Chinese Chemical Society and Institute of Materia Medica, Chinese Academy of Medical Sciences.

Atomically precise silver (Ag) clusters have emerged as a class of transformative nanomaterials applied in research fields of optics [1–3], catalysis [4–6], and biosensing [7–9], *etc*., which benefited from their well-defined atomic structures and tunable physicochemical properties [10–14]. Anions are well-known as templates to direct the formation of Ag clusters and control the shapes, sizes, and functions of the final products. Polyoxometalates (POMs) as a unique category of anionic metal-oxygen clusters [15–19], have been widely employed as structure-directing templates for intriguing Ag cluster assembly. Abundant oxygen coordination sites and high negative charge densities of POMs can induce the syntheses of high-nuclearity Ag clusters by functioning as either anionic templates [20–33] or surface-protecting ligands [34–42].

Organic ligands like thiolates [20,22,23,25,26] and alkynyls [21,24,27] are typically incorporated to enhance the structural stability in the POM-templated synthesis of Ag clusters, whereas phosphine ligands are rarely utilized as sole stabilizer in anionic templating synthetic processes. In contrast to the well-established applications of lacunary $[SiW_9O_{34}]^{9-}$ ({SiW_9O_{34}}) [29–31] and $[PW_9O_{34}]^{9-}$ ({PW_9O_{34}}) [32,33], the employment of lacunary $[SbW_9O_{33}]^{9-}$ ({SbW_9O_{33}}) as an anionic structure-directing unit remains unexplored. In addition, our recently reported work revealed that the lacunary {SbW_9O_{33}} can *in situ* generate isomeric bowl-shaped $[Sb_3W_{30}O_{105}]^{21-}$ ({$Sb_3W_{30}O_{105}$}) multidentate O-donating ligands, which will further induce and stabilize the structurally isomerized $\{Ag_{14}\}^{10+}$ clusters [34]. Therefore, we expect that the lacunary {SbW_9O_{33}} combined with organophosphine ligands may construct Ag clusters with aesthetic structures and interesting physicochemical properties, which can work as an ideal platform for studying the structure-property relationship.

Herein, we have successfully prepared four structurally similar Ag clusters, $Ag_{18}(SbW_9O_{33})_2(DPPP)_8$ (**1**), $Ag_{18}(SbW_9O_{33})_2(DPPB)_8$ (**2**), $Ag_{18}(SbW_9O_{33})_2(DPPPe)_8$ (**3**), and $Ag_{18}(SbW_9O_{33})_2(TPP)_{14}$ (**4**), by using a facile solvothermal approach in the presence of lacunary {SbW_9O_{33}} as structural-directing anionic template and external phosphine ligands. Single-crystal X-ray diffraction (SCXRD) analyses reveal that although four Ag clusters show similar sandwich-type geometries, subtle differences in peripheral phosphine ligands have rendered them with distinct photoluminescent, catalytic, and photothermal conversion performance.

The synthetic approaches of four Ag clusters were identical except for the use of different external phosphine ligands, and the syntheses of four Ag clusters are reproducible with decent product yields (see Supporting information for the detailed synthetic procedure). Briefly, compound **1** was synthesized *via* a one-pot solvothermal reaction of CH_3COOAg, TBA–{SbW_9O_{33}}, and DPPP ligand in a CH_3CN/DMF mixed solvent system at 80 °C for 24 h. Multiple attempts to obtain target products at ambient condi-

* Corresponding authors.
E-mail addresses: landeng@bit.edu.cn (L. Deng), liutf@bit.edu.cn (T. Liu), hlv@bit.edu.cn (H. Lv).

https://doi.org/10.1016/j.cclet.2025.111416
1001-8417/© 2026 Published by Elsevier B.V. on behalf of Chinese Chemical Society and Institute of Materia Medica, Chinese Academy of Medical Sciences.

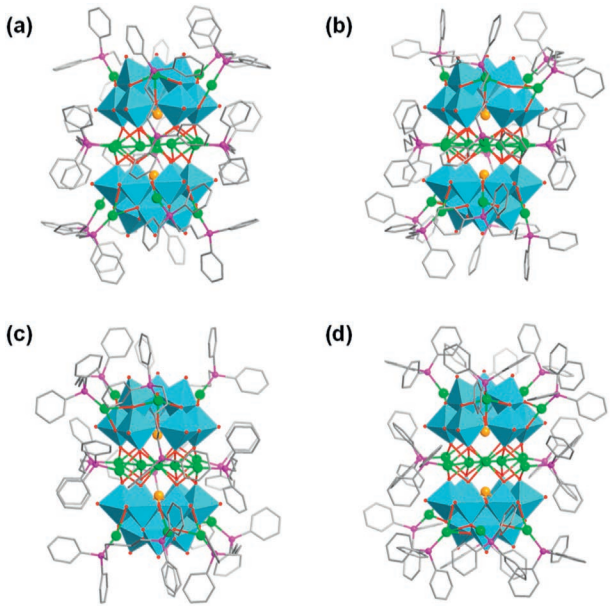


Fig. 1. Overall structures of compounds (a) **1**, (b) **2**, (c) **3**, and (d) **4**, respectively. Color codes: Ag, green; W, blue; Sb, orange; P, purple; C, gray; O, red; {WO_6}, blue polyhedron.

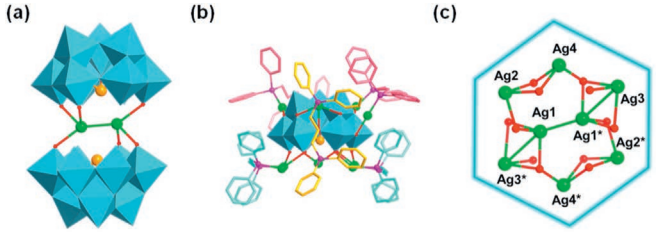


Fig. 2. (a) Fragment structure of {$Ag_2(SbW_9O_{33})_2$} in compound **1**. (b) Coordination modes of partial surface DPPP ligands in compound **1**. (c) The arrangement of Ag atoms in the central belt layer. Color codes: Ag, green; W, blue; Sb, orange; P, purple; C, pink, cyan, yellow; O, red; {WO_6}, blue polyhedron.

tions were unsuccessful, indicating the importance of solvothermal treatment process. It is also noted that both the solvent system and the ratios of reactants are crucial factors for the successful formation of crystals **1**–**4**, otherwise only precipitates were formed.

Given their similar geometric structures, only compound **1** was selected as a representative for the detailed structural description. Single crystal X-ray diffraction (SCXRD) analysis revealed that the charge-neutral compound **1** crystallized in the triclinic $P\bar{1}$ space group ($a = 20.4$ Å, $b = 21.3$ Å, $c = 23.2$ Å, $\alpha = 86.537°$, $\beta = 64.578°$, $\gamma = 62.903°$) (Table S1 in Supporting information, CCDC deposition number: 2428232). Structural interpretation suggested that compound **1** adopted a {SbW_9O_{33}}-sandwiched configuration, which consists of 8 $\{Ag_2(DPPP)_2\}^{2+}$ cations and one {$Ag_2(SbW_9O_{33})_2$} unit (Figs. 1a and 2a). The structure of {$Ag_2(DPPP)_2$} was commonly reported in the literatures [5,35,43] with Ag–P bond distances ranging from 2.324(9)–2.404(0) Å (Table S3 in Supporting information). While the {$Ag_2(SbW_9O_{33})_2$} unit adopted a sandwich-type geometry, featuring a central {Ag_2} pair bridged by two trilacunary {SbW_9O_{33}} POM ligands in an antiparallel orientation. The surrounding DPPP ligands connected the {$Ag_2(SbW_9O_{33})_2$} framework in three locations through μ_1 coordination mode (Fig. 2b). Four DPPP ligands are located at the edge of {SbW_9O_{33}} (the carbon atom is highlighted in pink), the other two are situated at the sandwich waist (marked with cyan) and another two are spanned each {SbW_9O_{33}} ligand (marked with yellow) with Ag–$O_{\mu 2}$ bonds ranging from 2.365(9) Å to 2.666(0) Å (Table S3 in Supporting information). Ag atoms in the sandwich layer are connected by oxygen atoms, showing a pseudo hexagonal arrangement (Fig. 2c). The packing diagram of compound **1** in *c*-axis direction is supplemented in Fig. S2 (Supporting information), implying phosphine ligands could contribute to the formation of discrete cluster.

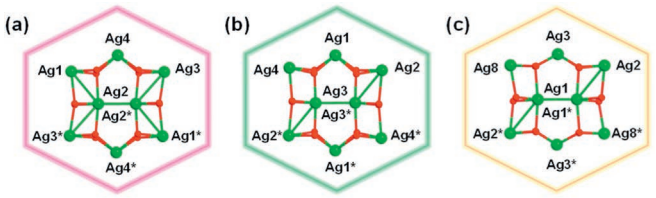


Fig. 3. The arrangement of Ag atoms in the central belt layer for compounds (a) **2**, (b) **3**, and (c) **4**, respectively. Color codes: Ag, green; O, red.

The crystallographic data and structural refinements for compounds **2**–**4** are listed in Table S1 (CCDC deposition numbers: 2428227, 2428229, and 2428230). Compounds **2** and **3** were crystallized in the triclinic $P\bar{1}$ space group (compound **2**: $a = 18.7$ Å, $b = 19.9$ Å, $c = 24.2$ Å, $\alpha = 109.810°$, $\beta = 97.620°$, $\gamma = 113.304°$; compound **3**: $a = 19.3$ Å, $b = 21.2$ Å, $c = 19.5$ Å, $\alpha = 80.952°$, $\beta = 66.692°$, $\gamma = 78.321°$), while compound **4** crystallized in monoclinic $P2_1/n$ space group (compound **4**: $a = 19.3$ Å, $b = 34.2$ Å, $c = 24.3$ Å, $\alpha = 90°$, $\beta = 109.940°$, $\gamma = 90°$). All three compounds adopted similar {SbW_9O_{33}}-sandwiched architectures to compound **1** except for the different spatial organization and coordination geometries of the encapsulated Ag atoms induced by different phosphine ligands (Figs. 1b-d). Specifically, Ag atoms in the central belt layers of compounds **2**–**4** exhibit a more ordered arrangement compared to that of compound **1** (Figs. 3a-c). Both DPPB and DPPPe adopted identical coordination geometries to DPPP ligands (Figs. S1d and e in Supporting information), while TPP ligands displayed an interesting arrangement with four of them occupying equatorial positions and the remaining ones being equally distributed over axial positions (Fig. S1f in Supporting information). For compounds **2**, **3**, and **4**, the Ag–Ag bond distances range from 2.743(6)–3.314(3), 2.882(0)–3.362(6), and 2.830(2)–3.371(5) Å; while the Ag–O bond distances range from 2.432(0)–2.582(1), 2.362(2)–2.572(0), and 2.311(4)–2.556(0) Å, and the distances of Ag–P bond are in the range of 2.324(0)–2.400(0), 2.305(2)–2.396(1), and 2.311(0)–2.361(2) Å, respectively (Tables S5, S7 and S9 in Supporting information). Moreover, the two-dimensional packing diagrams of compounds **2**, **3**, and **4** are available in Figs. S2-S5 (Supporting information), respectively. Fourier-transform infrared (FT-IR) spectra of compounds **1**–**4** revealed the characteristic vibrational modes, confirming the presence of phosphine ligands and the POM templates (Fig. S6 in Supporting information). X-ray photoelectron spectroscopy (XPS) analyses confirmed that the existence of Ag, W, Sb, P and O elements in the four clusters, and the high-resolution XPS spectra revealed two characteristic peaks at 368.5 and 374.5 eV corresponding to Ag $3d_{5/2}$ and Ag $3d_{3/2}$, respectively, revealing the oxidation state of Ag atoms were +1 in these compounds (Figs. S7-S10 in Supporting information). The bond valence sum (BVS) calculations determined that W and Sb are +6 and +3, respectively, which were consistent with the high-resolution XPS results (Tables S2, S4, S6, and S8 in Supporting information).

Then, the optical properties of compounds **1**–**4** have been systematically investigated. The solid-state UV–vis diffuse reflectance of compounds **1**–**4** exhibited broad absorption in the range of 400–600 nm, indicating their visible light absorption ability (Fig. S11 in Supporting information). The solid-state four clusters showed no detectable emission at room temperature upon excita-

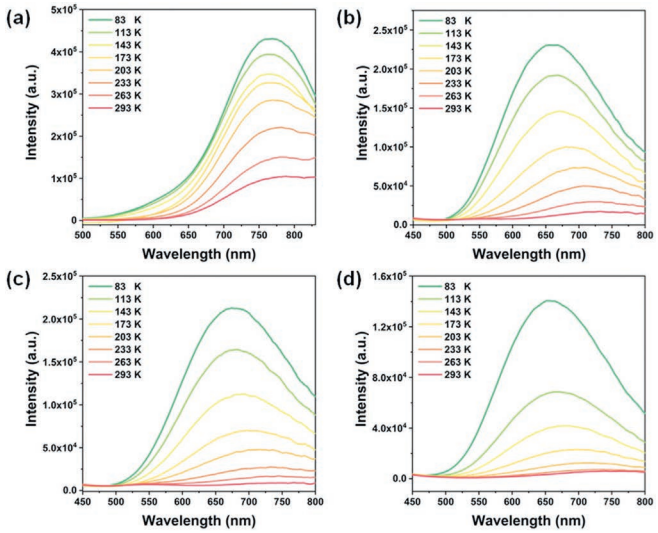


Fig. 4. Temperature-dependent photoluminescence spectra of compounds (a) **1**, (b) **2**, (c) **3**, and (d) **4** at 83–293 K, respectively.

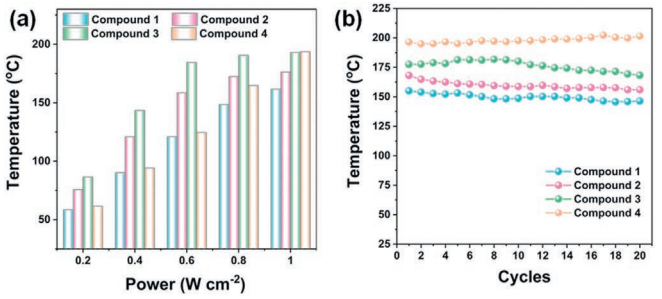


Fig. 5. (a) Photothermal conversion of compounds **1**–**4** at different powers under 465 nm laser irradiation. (b) Stability study of these four clusters for 20 successive photothermal cycles.

tion by the hand-held UV lamp ($\lambda_{ex} = 365$ nm). In contrast, they displayed bright red emission at cryogenic (83 K) temperatures. Thus, the temperature-dependent emission spectra of solid-state powders **1**–**4** were recorded in a temperature range of 83–293 K with 30 K as an interval in Fig. 4. Compound **1** exhibited a stable emission maximum at ~764 nm throughout the cooling process from 293 K to 83 K in Fig. 2a. The emission intensity showed a linear negative temperature dependence (Fig. S12a in Supporting information), resulting from enhanced molecular rigidity and suppressed non-radiative decay pathways at lower temperatures [44–46], further suggesting its promising application as molecular luminescent thermometer. The emission intensity of compound **1** exhibited a 4-fold enhancement at 83 K compared to ambient condition, demonstrating a linear temperature-response relationship. Furthermore, the photoluminescence lifetime of compound **1** was 119.3 μs at 83 K (Fig. S13 in Supporting information), revealing the phosphorescent nature of emission. In addition, the photoluminescence spectra of compounds **2**, **3**, and **4** displayed maximum emission of 698, 698, and 734 nm at 293 K (Figs. 4b-d). Notably, these emission peaks exhibited significant blue shifts to 660, 654, and 669 nm at 83 K (Figs. 4b-d and Figs. S12b-d in Supporting information), respectively. The observed blue-shift phenomenon may originate from the progressively restricted mobility of the organic phosphine ligands at lower temperatures [47]. The emission intensity performed perfect single exponential temperature dependence (Figs. S12b-d), with compounds **2**, **3**, and **4** exhibiting dramatic emission enhancement by 13-, 17-, and 19-fold at 83 K compared to their room-temperature intensities, manifesting a temperature-dependent photoluminescence behavior. Furthermore, the photoluminescence lifetimes of these three clusters were measured to be 51.6, 58.6, and 31.4 μs at 83 K (Figs. S14-S16 in Supporting information), respectively.

Extensive studies have confirmed that emission quenching in photothermal materials can significantly enhance their light-to-heat conversion efficiencies by favoring non-radiative relaxation pathways [48,49]. Ag clusters represent promising candidates for solar energy conversion systems due to their outstanding broadband light-harvesting properties and efficient photothermal conversion performance [29–31,50–54]. The observed weak room-temperature photoluminescence of compounds **1**–**4** prompted further investigation of their photothermal conversion properties. The photothermal conversion nature of these four compounds in crystalline states were evaluated extensively with different power densities under 465 nm laser irradiation in Fig. 3. It is found that the photothermal conversion efficiency also depended on the laser power density, with the maximum temperatures increasing proportionally with the elevated power density. As the power density increased, the platform temperature of four compounds raised quickly, reached at 161.7, 176.3, 193.1, and 193.6 °C at 1.0 W/cm^2, respectively (Fig. 5a). The long-term stability tests of 50-s on-off were explored at the power density of 0.3, 0.6, and 0.9 W/cm^2, respectively (Figs. S17a, S18a, S19a, and S20a in Supporting information). The platform temperatures of compounds **1**–**4** can be stabilized at 81, 100, 118, and 79 °C with 0.3 W/cm^2 power density, respectively. At the power density of 0.9 W/cm^2, the platform temperatures further increased up to 166, 179, 183, and 189 °C, respectively, demonstrating strong power-dependent behavior.

The photothermal recycling stabilities of four Ag clusters were investigated by reversible ON–OFF cycles under 465 nm laser irradiation at 0.9 W/cm^2 for 20 successive photothermal cycles (Fig. 5b, Figs. S17b, S18b, S19b, and S20b in Supporting information). The platform temperature of compounds **1**–**4** exhibited minor variations during cycles and the FT-IR spectra have further confirmed that the molecular structures of all four compounds remained largely unchanged after the photothermal processes (Figs. S17d, S18d, S19d, and S20d in Supporting information), showing the excellent photothermal recyclability and stability. Compared to the previously reported POM-templated Ag clusters, compounds **1**–**4** exhibited decent photothermal conversion performance with rapid photothermal conversion rate and high recyclability (Table S10 in Supporting information). Near-infrared (NIR) thermal images have captured the real-time temperature profiles of the samples at corresponding irradiation time (Figs. S17c, S18c, S19c, and S20c in Supporting information), revealing the rapid and efficient light-to-heat conversion of the four Ag clusters. The heating rates of compounds **1**–**4** were 23.4, 24.5, 23.6, and 29.9 °C/s, respectively. Among these, compound **4** showed optimal photothermal conversion performance, which should be attributed to its lowest emission intensity under ambient condition, thereby leading to the most dominant nonradiative relaxation process to generate heat.

Then, the reduction of 4-nitrophenol (4-NP) to 4-aminophenol (4-AP) using $NaBH_4$ was selected as model reaction to evaluate the catalytic performance of four compounds (Fig. 6a), and real-time monitored by UV–vis absorption spectroscopy. After adding catalysts to the mixture of 4-NP and $NaBH_4$ (see Supporting information for the detailed experimental procedure), the absorption peaks of 4-NP at 400 nm quickly disappeared along with the increase of the absorption band at 300 nm showing the formation of product 4-AP. In Fig. 6b, it is found that compound **1** has exhibited the highest catalytic activity, achieving complete conversion within just 5 min (Fig. S21a in Supporting information). In contrast, it will

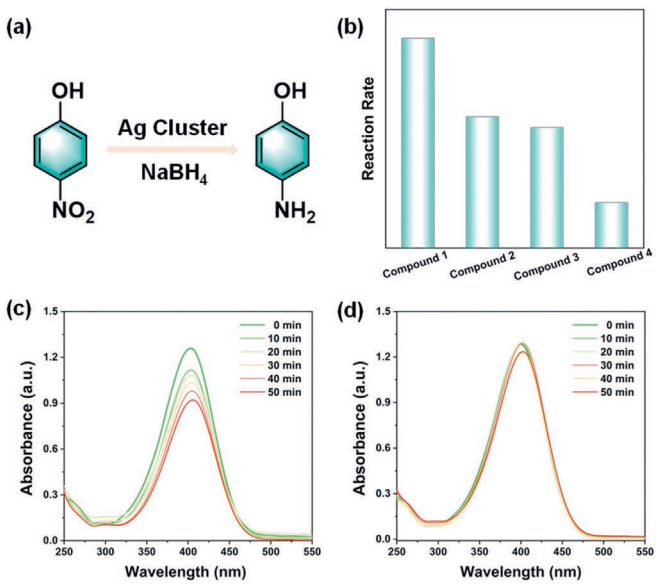


Fig. 6. (a) Schematic illustration of the model reaction for the 4-NP reduction. (b) Comparison for reaction rate. Time-dependent UV–vis absorption spectra of 4-NP reduction using (c) TBA–{SbW_9O_{33}} catalyst and (d) blank test, respectively.

take 7 min for compounds **2** (Fig. S22a in Supporting information) and **3** (Fig. S23a in Supporting information), and 20 min for compound **4** to achieve the complete conversion of 4-NP, respectively (Fig. S24a in Supporting information). The plot of $\ln(C_t/C_0)$ (C_0 is the initial concentration of 4-NP and C_t is the concentration at reaction time t) against reaction time indicated that the reduction of 4-NP followed first-order kinetics, and the calculated apparent rate constants k for the compounds **1**–**4** were 0.792, 0.496, 0.455, and 0.127 min^{-1}, respectively (Figs. S21b, S22b, S23b and S24b in Supporting information). In addition, a series of control experiments (TBA-{SbW_9O_{33}} catalyst *vs.* catalyst-free condition) showed that these comparative catalysts exhibited very low or negligible catalytic activities for the 4-NP reduction (Figs. 6c and d), highlighting the essential role of Ag clusters in the 4-NP reduction process. The observed differences in catalytic activity are primarily attributed to the structural variations of compounds **1**–**4**. It is proposed that the increased steric hindrance from DPPP to TPP ligands can prohibit the free accessibility to the active Ag sites, thereby slowing down the substrate adsorption and hydrogen transfer process for efficient catalysis according to the Langmuir–Hinshelwood (LH) kinetic model [55,56].

In summary, we have successfully synthesized four {SbW_9O_{33}}-sandwiched Ag clusters by using a facile solvothermal approach, where the structures of four Ag clusters can be controlled by adjusting the external phosphine ligands. All four Ag clusters displayed intriguing temperature-dependent photoluminescence behaviors and promising photothermal conversion abilities with excellent stability and recyclability. Moreover, compound **1** has shown superior ability to catalyze the reduction of 4-NP with rate constant of 0.792 min^{-1}. This work not only enriches the structural diversity of Ag clusters by introducing lacunary {SbW_9O_{33}} ligands, but also sheds light on the exploration of their optical and catalytic properties in various research fields.

CRediT authorship contribution statement

Wanting Sun: Writing – original draft, Validation, Software, Investigation, Formal analysis, Data curation. **Lan Deng:** Writing – original draft, Validation, Formal analysis, Data curation. **Mengyun Zhao:** Visualization, Validation, Software. **Tianfu Liu:** Writing – original draft, Supervision, Resources, Project administration, Funding acquisition. **Hongjin Lv:** Writing – review & editing, Supervision, Project administration, Funding acquisition, Conceptualization.

Declaration of competing interest

The authors declare that they have no known competing financial interests or personal relationships that could have appeared to influence the work reported in this paper.

Acknowledgments

This work is financially supported by the National Natural Science Foundation of China (No. 22471017), the Recruitment Program of Global Experts (Young Talents) and BIT Excellent Young Scholars Research Fund. The instrumental support from the Analysis and Testing Center of Beijing Institute of Technology is also highly appreciated.

Supplementary materials

Supplementary material associated with this article can be found, in the online version, at doi:10.1016/j.cclet.2025.111416.

References

[1] J.S. Yang, M.M. Zhang, Z. Han, et al., Chem. Commun. 56 (2020) 2451–2454.
[2] S.S. Zhang, S. Havenridge, C. Zhang, et al., J. Am. Chem. Soc. 144 (2022) 18305–18314.
[3] Y. Feng, X. Jing, F. Fu, et al., Sci. China Chem. 68 (2025) 580–589.
[4] Z.J. Guan, R.L. He, S.F. Yuan, et al., Angew. Chem. Int. Ed. 61 (2022) e202116965.
[5] S.F. Yuan, Z.J. Guan, Q.M. Wang, J. Am. Chem. Soc. 144 (2022) 11405–11412.
[6] H. Shen, Q. Zhu, J. Xu, et al., Nanoscale 15 (2023) 14941–14948.
[7] R.K. Gupta, L. Li, Z. Wang, et al., Chem. Sci. 14 (2023) 1138–1144.
[8] J.Y. Wang, J.W. Yuan, X.M. Liu, et al., Aggregate 5 (2024) e508.
[9] Z. Wang, Y.J. Zhu, O. Ahlstedt, et al., Angew. Chem. Int. Ed. 63 (2024) e202314515.
[10] Y. Du, H. Sheng, D. Astruc, et al., Chem. Rev. 120 (2020) 526–622.
[11] X. Kang, Y. Li, M. Zhu, et al., Chem. Soc. Rev. 49 (2020) 6443–6514.
[12] Y.P. Xie, Y.L. Shen, G.X. Duan, et al., Mater. Chem. Front. 4 (2020) 2205–2222.
[13] B. Yin, Z. Luo, Coord. Chem. Rev. 429 (2021) 213643.
[14] M.F. Matus, H. Häkkinen, Nat. Rev. Mater. 8 (2023) 372–389.
[15] H. Lv, W. Guo, K. Wu, et al., J. Am. Chem. Soc. 136 (2014) 14015–14018.
[16] Y. Chen, H.P. Wu, Z.W. Guo, et al., Chin. Chem. Lett. 36 (2025) 110552.
[17] M. Chi, Y. Zeng, Z.L. Lang, et al., ACS Catal. 14 (2024) 5006–5015.
[18] L.M. Cui, W.H. Fang, J. Zhang, Chin. Chem. Lett. 36 (2025) 110386.
[19] J. Li, Y. Feng, F. Fu, et al., Chin. Chem. Lett. 35 (2024) 108736.
[20] J.Y. Shi, R.K. Gupta, Y.K. Deng, et al., Polyoxometalates 1 (2022) 9140010.
[21] L. Li, Y. Zhu, B. Han, et al., Chem. Commun. 58 (2022) 9234–9237.
[22] Y.H. Xia, X.Y. Xia, J.J. Fang, et al., Dalton Trans. 51 (2022) 14557–14562.
[23] W. Biao, X.X. Li, S.T. Zheng, et al., Chem. Commun. 59 (2023) 2927–2930.
[24] C. Ma, K. Gui, J. Xu, et al., Inorg. Chem. 62 (2023) 20980–20986.
[25] K. Sheng, Z. Wang, L. Li, et al., J. Am. Chem. Soc. 145 (2023) 10595–10603.
[26] R. Ge, P.W. Cai, C. Sun, et al., Chem. Sci. 15 (2024) 12543–12549.
[27] Z. Zhao, M. Zhao, L. Deng, et al., Chem. Commun. 60 (2024) 5415–5418.
[28] R. Ge, X.X. Li, S.T. Zheng, Coord. Chem. Rev. 435 (2021) 213787.
[29] Q. Li, F. Fu, M. Zhao, et al., Chin. Chem. Lett. 36 (2025) 110090.
[30] J. Zhang, Y. Dong, L. Deng, et al., Nanoscale 16 (2024) 11518–11523.
[31] K. Sheng, B.L. Han, Z. Wang, et al., Angew. Chem. Int. Ed. 64 (2025) e202416065.
[32] Z.G. Jiang, K. Shi, Y.M. Lin, et al., Chem. Commun. 50 (2014) 2353–2355.
[33] Z. Wang, Y.J. Zhu, Y.Z. Li, et al., Nat. Commun. 13 (2022) 1802.
[34] M. Chi, J. Wei, Z. Zhao, et al., Angew. Chem. Int. Ed. 64 (2025) e202424499.
[35] Y. Feng, F. Fu, L. Zeng, et al., Angew. Chem. Int. Ed. 63 (2024) e202317341.
[36] L.H. Hong, S.N. Yue, X. Huang, et al., Angew. Chem. Int. Ed. 63 (2024) e202404314.
[37] K. Yonesato, D. Yanai, S. Yamazoe, et al., Nat. Chem. 15 (2023) 940–947.
[38] K. Yonesato, H. Ito, D. Yokogawa, et al., Angew. Chem. 132 (2020) 16503–16507.
[39] K. Yonesato, H. Ito, H. Itakura, et al., J. Am. Chem. Soc. 141 (2019) 19550–19554.
[40] C.H. Zhan, J.M. Cameron, J. Gao, et al., Angew. Chem. Int. Ed. 53 (2014) 10362–10366.
[41] Y. Kikukawa, Y. Kuroda, K. Suzuki, et al., Chem. Commun. 49 (2013) 376–378.
[42] Y. Kikukawa, Y. Kuroda, K. Yamaguchi, et al., Angew. Chem. Int. Ed. 51 (2012) 2434–2437.
[43] G.X. Duan, J. Han, B.Z. Yang, et al., Nanoscale 12 (2020) 1617–1622.
[44] M.A. Omary, H.H. Patterson, Inorg. Chem. 37 (1998) 1060–1066.
[45] J. Zheng, Y.D. Yu, F.F. Liu, et al., Chem. Commun. 50 (2014) 9000–9002.

[46] N. Mirzadeh, S.H. Privér, A.J. Blake, et al., Chem. Rev. 120 (2020) 7551–7591.
[47] V.W.W. Yam, V.K.M. Au, S.Y.L. Leung, Chem. Rev. 115 (2015) 7589–7728.
[48] Q. Lu, X. Wang, Adv. Sci. 9 (2021) 2104225.
[49] X. Cui, Q. Ruan, X. Zhuo, et al., Chem. Rev. 123 (2023) 6891–6952.
[50] Z. Wang, L. Li, L. Feng, et al., Angew. Chem. Int. Ed. 61 (2022) e202200823.
[51] K. Sheng, Z. Wang, L. Li, et al., J. Am. Chem. Soc. 145 (2023) 10595–10603.
[52] Z. Wang, Y.J. Zhu, B.L. Han, et al., Nat. Commun. 14 (2023) 5295.
[53] Z. Wang, Y.J. Zhu, O. Ahlstedt, et al., Angew. Chem. Int. Ed. 63 (2024) e202314515.
[54] Z. Wang, Y.C. Wang, T.Y. Xu, et al., Angew. Chem. Int. Ed. 63 (2024) e202403464.
[55] S. Wunder, F. Polzer, Y. Lu, et al., J. Phys. Chem. C 114 (2010) 8814–8820.
[56] P. Zhao, X. Feng, D. Huang, et al., Coord. Chem. Rev. 287 (2015) 114–136.